

Effect of Boundary Layer Evolution on Nitrogen Dioxide (NO₂) and Formaldehyde (HCHO) Concentrations at a High-altitude Observatory in Western India

Mriganka Sekhar Biswas^{1,2}, G. Pandithurai¹, M.Y. Aslam¹, Rohit D. Patil¹, V. Anilkumar¹, Shrikant D. Dudhambe¹, Christophe Lerot³, Isebel De Smedt³, Michel Van Roozendael³, Anoop S. Mahajan^{1*}

¹ Indian Institute of Tropical Meteorology, Ministry of Earth Sciences, Pune, India

² Savitribai Phule Pune University, Pune, India

³ Belgian Institute for Space Aeronomy, Brussels, Belgium

ABSTRACT

Nitrogen dioxide (NO₂) and formaldehyde (HCHO) are some of the most important trace gases in the atmosphere, acting as precursors for ozone formation and as pollutants at high concentrations. Although several observations of these species have been reported in the boundary layer, observations at high altitude sites are limited, especially in India. This study reports observations of NO₂ and HCHO using the Multi AXis Differential Optical Absorption Spectroscopy (MAX-DOAS) technique at the High Altitude Cloud Physics Laboratory (HACPL), Mahabaleshwar in the rural Western Ghats region of India. Measurements were conducted during the pre-monsoon season between 25th April and 30th May 2018. The average NO₂ mixing ratio was 0.19 ± 0.06 ppb (range: 0.03 ppb to 0.69 ppb). Typically, NO₂ mixing ratios were found to increase from early in morning and reached a maximum in the afternoon, contrary to an expected diurnal profile dominated by photochemistry. The average HCHO mixing ratio was 1.6 ± 0.61 ppb (range: 0.16 ppb–4.5 ppb). HCHO mixing ratios also showed an increase from early in the morning and reach a maximum at ~3 pm in the afternoon after which a decrease was observed, peaking much later than expected from a photochemistry dominated profile. Using observations of the boundary layer height, back trajectories and the known photochemistry, we conclude that the observed diurnal variation in these two species is dominated by the mixing of emissions from the base of the mountain, resulting from the evolution of the boundary layer at the HACPL site.

Keywords: Formaldehyde (HCHO), Nitrogen dioxide (NO₂), Boundary Layer (BL), India, Western Ghats

OPEN ACCESS

Received: May 4, 2020

Revised: November 6, 2020

Accepted: November 16, 2020

* Corresponding Author:


anoop@tropmet.res.in

Publisher:

Taiwan Association for Aerosol
Research

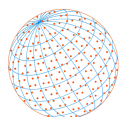
ISSN: 1680-8584 print

ISSN: 2071-1409 online

 **Copyright:** The Author(s). This is an open access article distributed under the terms of the [Creative Commons Attribution License \(CC BY 4.0\)](https://creativecommons.org/licenses/by/4.0/), which permits unrestricted use, distribution, and reproduction in any medium, provided the original author and source are cited.

1 INTRODUCTION

Trace gases constitute less than 0.1% of the atmosphere (by volume) but affect air quality, participate in reactive atmospheric chemistry and cause changes in the global radiation budget. Formaldehyde (HCHO) is an oxidation product of various higher volatile organic compounds (VOCs) and participates in ozone (O₃) formation. HCHO is also an atmospheric pollutant (EPA, 2015) that plays a crucial role in tropospheric O₃ formation (Carter and Atkinson, 1987). Hence observations and studies of HCHO are important for both air quality and understanding of atmospheric chemistry. Being an oxidation product of various VOCs, HCHO is the most abundant carbonyl compound in the atmosphere (Hak *et al.*, 2005 and references therein). This is why HCHO can be used as a tracer for the study of various VOCs and their sources. Although biogenic VOCs are the main sources of atmospheric HCHO (Carlier *et al.*, 1986; Fu *et al.*, 2007; Smedt *et al.*

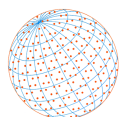


et al., 2010); pyrogenic and anthropogenic sources are also important (Herndon *et al.*, 2005; Zhu *et al.*, 2017). Photolysis and oxidation by OH radicals are the main decomposition processes (Lowe and Schmidt, 1983), whereas dry and wet depositions are also important for its removal (Atkinson, 2000). Considering the impact of HCHO on air quality and atmospheric chemistry, long term observations of HCHO are important to understand its spatial and temporal variability. Using OMI data and GEOS-Chem model simulations, Surl *et al.* (2018) reported that the seasonal cycle of HCHO columns over India is highly correlated with variations in surface temperature. Hence, they concluded that the HCHO variability over India is controlled by biogenic emissions rather than anthropogenic emissions. Dutta *et al.* (2010) reported a summertime averaged HCHO concentration of $23.64 \pm 12.16 \mu\text{g m}^{-3}$ (19.3 ± 9.9 ppb) from Kolkata in Eastern India during 2007–2008. They also reported a prominent peak in HCHO concentrations from 11 am to 2 pm due to vehicular emissions. Khare *et al.* (1997) reported an averaged HCHO mixing ratio of 1.4 ± 0.8 ppb (range: 0.3–4.2 ppb) with a peak at ~10 am at a rural site in the IGP region during monsoon 1995–1996. In another study Khare *et al.* (1997b) reported an average 0.8 ± 0.5 ppb (ranging 0.2–2.8 ppb) HCHO in a semiarid region in northern India, with a peak in the afternoon at ~3–7 pm during February, 1995. Recently Sarkar *et al.* (2017) reported annually averaged HCHO concentrations of $11.6 \pm 16.3 \mu\text{g m}^{-3}$ (9.5 ± 13.3 ppb) at a low populated eastern Himalayan hill station in Darjeeling. Hoque *et al.* (2018) reported HCHO mixing ratios ranging between 2–6 ppb at a semi-urban location in the IGP for the year 2017. Biswas *et al.* (2019) reported an average daytime HCHO mixing ratio of 1.93 ± 0.60 ppb at a rural site in the IGP region during the monsoon period of 2014 (June–September). They observed a diurnal profile peaking between 10 am to 12 pm, as would be expected with photochemical production from precursor VOCs. The past observations of HCHO over India are presented in Table 1.

Nitrogen dioxide (NO₂) is also an important component of tropospheric O₃ synthesis process (Crutzen, 1974). NO₂ in the atmosphere acts as an oxidant and changes the hydroxyl radical (OH) concentration through reactive photochemistry (Levy, 1971). As an atmospheric pollutant, NO₂ is responsible for various health hazards (Burnett *et al.*, 2004; WHO, 2013), acid rain and nitrate aerosol formation. Major natural sources of NO₂ are lightning, forest fires and soil microbial processes (Zhang *et al.*, 2003; Jaeglé *et al.*, 2005; Schumann and Huntrieser, 2007). High temperature fossil fuel combustion, industries, thermal power plants, automobiles and biomass burning are the main anthropogenic sources. Conversion to nitric acid (HNO₃) during the daytime, dinitrogen pentoxide (N₂O₅) hydrolysis during the nighttime, transport and dry depositions are the main sinks for NO₂ (Finlayson-Pitts and Pitts, 2000; Jacob, 2000). Using surface in-situ observations from the Indian Central Pollution Control Board (CPCB), Mallik and Lal (2014) studied the seasonal variability of NO₂ in 6 Indian cities (Delhi, Jodhpur, Kolkata, Guwahati, Durgapur and Nagpur) and found that the winter time NO₂ concentration is highest for most Indian urban regions (except Jodhpur). Renuka *et al.* (2014) reported NO_x (NO₂ + NO) observations from Gadanki, a rural site in Southern India for the year 2010–11 with NO_x concentrations in the range 0.5–2 ppb. Hoque *et al.* (2018) reported NO₂ mixing ratios ranging between 0.5–1.5 ppb at a semi-urban location in the Indo-Gangetic Plain (IGP) for the year 2017, with the highest value in June and the lowest value in August. Sarangi *et al.* (2013) have reported an average NO₂ mixing ratio of 2.2 ± 2 ppb during May, 2009–11 at a high altitude Himalayan station in Nainital, India, showing diurnal variation dominated by anthropogenic emissions with traffic peaks clearly visible. Naja *et al.* (2003) reported observations of NO and NO_x (NO + NO₂) along with O₃ at Mt. Abu, a high altitude site in the western India. They reported that O₃ destruction took place in the afternoon, with NO concentrations increasing,

Table 1. HCHO observations from India.

Authors	Place of observation	Year of observation	HCHO observations
Dutta <i>et al.</i> (2010)	Kolkata	2007–2008	$23.64 \pm 12.16 \mu\text{g m}^{-3}$ (19.3 ± 9.9 ppb)
Khare <i>et al.</i> (1997)	rural IGP region	monsoon 1995–1996	1.4 ± 0.8 ppb (range: 0.3–4.2 ppb)
Khare <i>et al.</i> (1997b)	semiarid region in northern India	February, 1995	0.8 ± 0.5 ppb (ranging 0.2–2.8 ppb)
Sarkar <i>et al.</i> (2017)	eastern Himalayan hill station in Darjeeling	June 2012–May 2013	$11.6 \pm 16.3 \mu\text{g m}^{-3}$ (9.5 ± 13.3 ppb)
Hoque <i>et al.</i> (2018)	semi-urban the IGP	2017	2–6 ppb
Biswas <i>et al.</i> (2019)	rural IGP	monsoon period of 2014	1.93 ± 0.60 ppb

**Table 2.** NO₂ (and NO_x) observations from rural and remote India.

Authors	Place of observation	Year of observation	HCHO observations
Renuka <i>et al.</i> (2014)	from Gadanki, a rural site in Southern India	2010–11	0.5–2 ppb (NO _x)
Hoque <i>et al.</i> (2018)	semi-urban the IGP	2017	0.5–1.5 ppb
Sarangi <i>et al.</i> (2013)	high altitude Himalayan station in Nainital	May, 2009–11	2.2 ± 2 ppb
Biswas <i>et al.</i> (2019)	rural IGP	monsoon period of 2014	0.81 ± 0.20 ppb

and hence the NO₂ would show a decrease due to photochemical destruction. Biswas *et al.* (2019) have reported an average daytime NO₂ mixing ratio of 0.81 ± 0.20 ppb from a rural site in IGP region during the monsoon period of 2014. Both Biswas *et al.* (2019) and Renuka *et al.* (2014) have reported a diurnal profile of NO₂ mixing ratios with a decrease in the morning and an increase in the late afternoon, which is due to photochemical loss of NO₂ during the daytime. NO₂ (and NO_x) observations over India are presented in Table 2.

In this paper we report simultaneous observations of NO₂ and HCHO from a high altitude site in the Western Ghats region of India. This is the first time these trace gas have been observed in this region, which is the most forested area in western India. Indeed, hitherto observations of atmospheric chemistry at high altitude site are rare all over the world (Okamoto and Tanimoto, 2016). The observations were made during the pre-monsoon period (April–May 2018). Using concurrent observations of aerosol optical depth (AOD), boundary layer height and back trajectories we try to understand the main drivers behind the diurnal variation of the traces gases and along with satellite observations identify the location of the sources in this region.

2 MEASUREMENT SITE AND METHODS

2.1 Measurement Site

Trace gas and other meteorological parameter measurements were conducted at the ‘High Altitude Cloud Physics Laboratory’ (HACPL) situated at Mahabaleshwar (Fig. 1), a hill station in the Western Ghats region of India. Mahabaleshwar is a town situated ~120 km south-west of a large city Pune and ~285 km south-east of the metropolis Mumbai in Western India. The town is surrounded by dense vegetation (Fig. 1(c)). The HACPL is situated on a mountain top plateau, at a height of 1378 m above mean sea level (17.92°N, 73.65°E). The base of the mountain is about 600 m above the sea level, meaning that the mountain plateau is approximately 800 m above the surrounding area. There is a rural settlement ~200 m southwest of the HACPL (Fig. 1(d)). The plateau stretches ~4 km towards the west; ~5 km towards the east; ~6 km towards the north and ~5 km towards the south of the measurement site. Due to the elevation of the plateau, the boundary layer remains below the HACPL site during the night. During the day, the boundary layer gradually rises above the HACPL site (further details are given in Section 4). There are a few small villages within a 25 km radius at the base of the mountain. About 9 km away on the east of HACPL site is a town named Panchgani and at 15 km is another town named large Wai. The synoptic scale wind direction over the HACPL site was found to be north-westerly and westerly during the campaign period, which was also confirmed using the back trajectory analysis (Figs. 1(e) and 1(f)).

2.2 Meteorological Observations and Boundary Layer Measurements

Observations of standard meteorological parameters (temperature, relative humidity, precipitation, wind direction, wind speed) were made throughout the study period and have been shown in Figs. 2(a)–2(e). The meteorological parameters were measured using an automatic weather station (WeatherPak®-2000), which was installed at a height of 10 m from the ground. In order to estimate the BL height at the measurement site, thermodynamic observations were carried out with a 35-channel (temperature, water vapor and liquid water profiler) ground-based microwave radiometer (MWR - MP-3000A developed by Radiometrics Corp., USA – further details can be found in Leena *et al.* (2015)). The MWR is composed of two radiofrequency subsystems. It has 58 vertical levels with 50 m resolution below 500 m, 100 m resolution between 500 m to 2000 m and 250 m resolution from 2000 m to 10000 m, with the time resolution of 4 minutes.

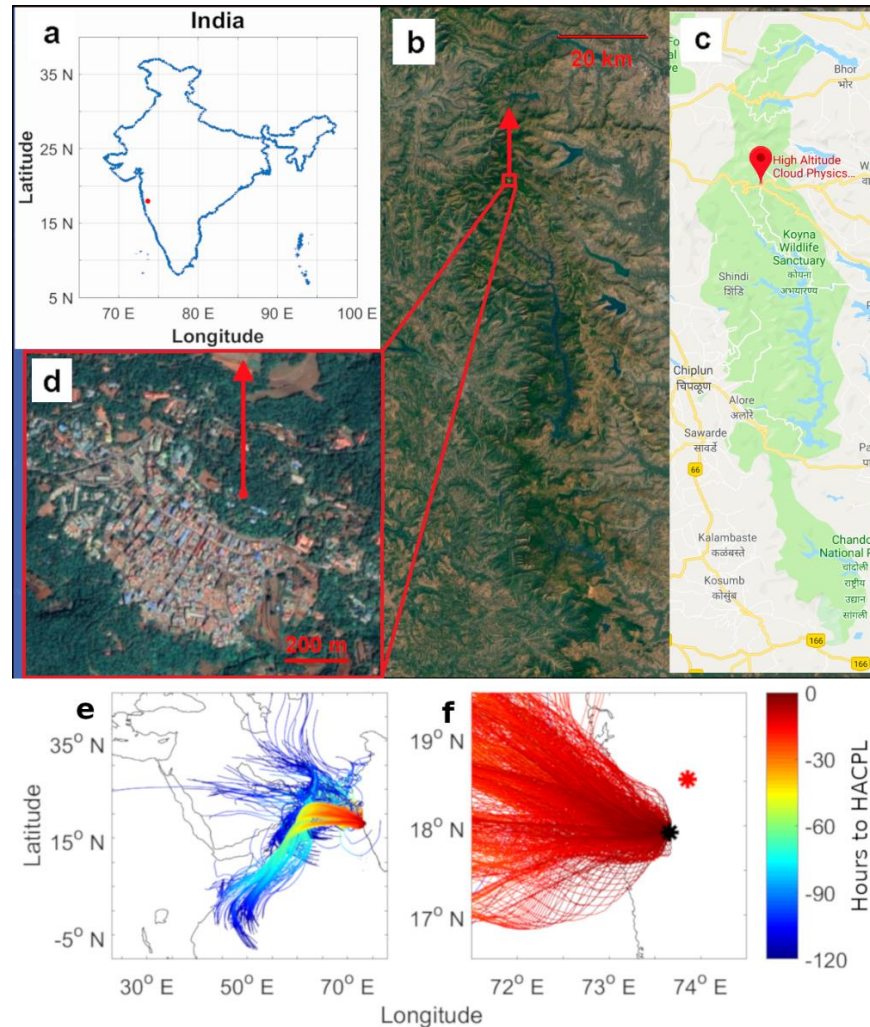
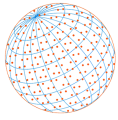


Fig. 1. The location of the measurement site at the High Altitude Cloud Physics Laboratory (HACPL) showing the nearby village and forested regions. Panel (a) represents the HACPL location in India. Panel (b) represents the HACPL location on a satellite map. Panel (c) shows the HACPL location using *Google Map*, where the green patch indicates the forested region. Panel (d) represents the zoomed in HACPL location on a *Google Satellite* image. Red arrows in panel (b) and (d) shows the viewing direction of the MAX-DOAS instrument. Panel (e) represents the 5-day air mass back trajectory reaching at HACPL site every hour during the campaign period. Panel (f) represents the zoomed in version of panel (e). Black asterisk (*) symbol on panel (f) indicate HACPL site, whereas red asterisk (*) indicate Pune city.

Atmospheric brightness temperature is measured at 14 frequencies in V-band ranging from 51 GHz to 59 GHz in oxygen absorption band for temperature observations and 21 K-band frequencies from 22 GHz to 30 GHz for water vapor observations. Liquid nitrogen and tip calibration of MWR was carried out periodically to ensure the data accuracy. This gave the height of the BL above the observation site throughout the campaign period. It should be noted that very low values close to zero indicate that the site was above the BL. A time series of the BL height at the HACPL site is presented in Fig. 2(f).

2.3 Trace Gas Measurements

Trace gases were measured using the Multi AXIS Differential Optical Absorption Spectroscopy (MAX-DOAS) technique. MAX-DOAS observations provide information of the trace gases averaged over several kilometers, in our case across the mountain ridge. This results in the observations being largely independent of any strong local sources and are hence more useful for studying

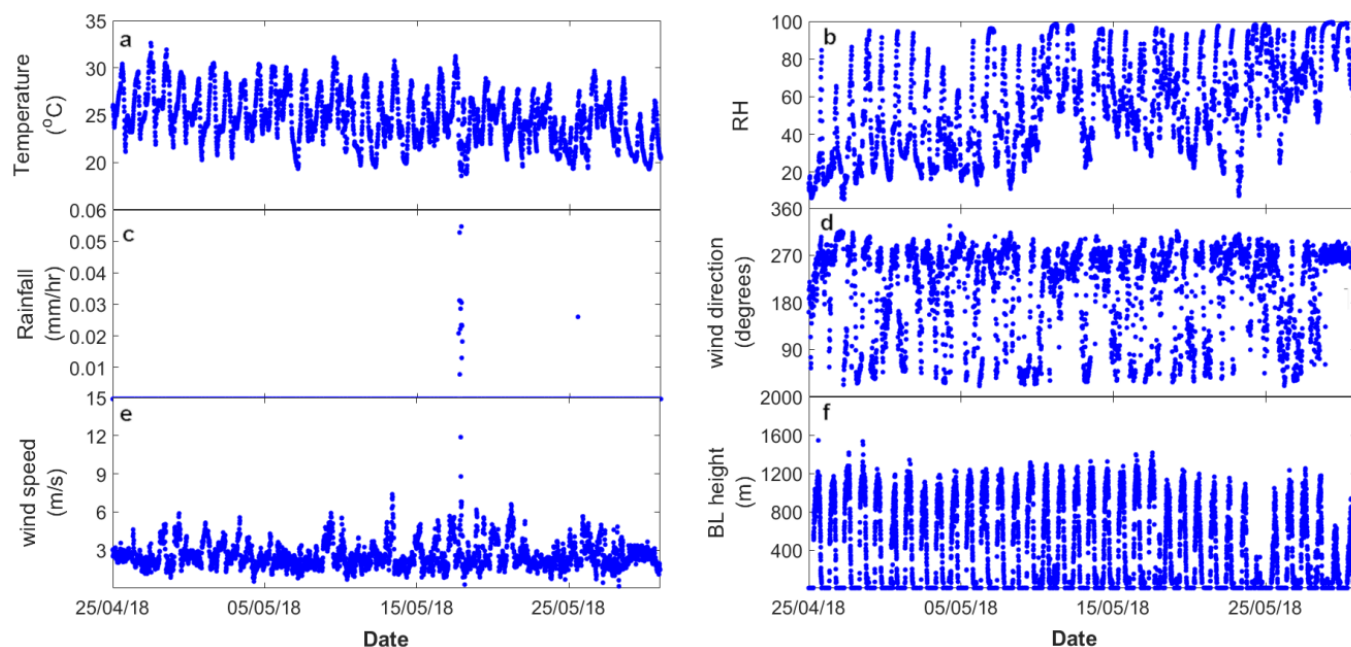
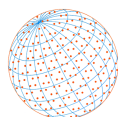
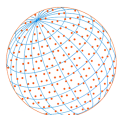


Fig. 2. Time series of various meteorological parameters measured during the campaign at HACPL. The panels on the plot represent the following parameters: (a) temperature, (b) relative humidity, (c) rainfall, (d) wind direction, (e) wind speed, (f) boundary layer height.

trace gas sources across the mountain ridge rather than at a single point. The MAX-DOAS (Envimes) instrument has two parts, one scanner unit (that directs scattered sunlight towards the spectrometer) and one indoor unit containing two different spectrometers. The scanner unit was installed on the rooftop of the HACPL building at a height of ~10 m above ground level. The scanner unit was pointed towards the geographical north overlooking the forest canopy. The spectrometer unit consists of two ultra-low stray light 75 mm Avantes spectrometers, both having a full width half maximum resolution of 0.7 nm and 100 μm slit. These two spectrometers measure solar spectra in two different wavelength ranges, UV: 301.50–463.73 nm and VIS: 443.54–584.19 nm. The same instrument has been used to measure HCHO and NO₂ in the Indian sub-continent in the past (Biswas *et al.*, 2019).

Scattered solar radiation spectra were measured at 10 different elevation angles (0°, 0.5°, 1°, 2°, 3°, 5°, 10°, 20°, 40° and 90°) per scan cycle. Spectra were recorded when the solar zenith angle (SZA) was less than 100°. The single exposure time per individual spectrum was set to 70% saturation of the charged coupled device (CCD) sensor. The field of view (FOV) of the instrument is 0.2°. The total exposure per elevation angle was set to 60 seconds for SZA less than 80°. For 80° < SZA < 90° and 90° < SZA < 100° the total exposure time was set to be 90 seconds and 120 seconds, respectively. The dark current, offset and mercury calibration spectra were recorded at the end of every day (when SZA > 100°). During post-processing, the spectra were calibrated using mercury emission lines which were recorded every day and with the Fraunhofer spectrum (Kurucz *et al.*, 1984). The spectra were also corrected for dark current and offset. Observations were made for the period 25th April, 2018 to 30th May, 2018. Due to instrumental problems, no data was recorded on three days 29th, April, 30th April and 21st May 2018. Observations at elevation angle 0° and 0.5° were started on 28th April and 2nd May, 2018, respectively. All the results from the campaign are reported in local time (Indian Standard Time).

The dark current and offset corrected spectra were then analyzed using the QDOAS spectral fitting software (Danckaert, 2014) (<http://uv-vis.aeronomie.be/software/QDOAS/>). Zenith spectra from each scan cycle were taken as a reference to remove the stratospheric contribution in the off-axis measurements (Hönninger *et al.*, 2004). HCHO differential slant column densities (DSCDs) were retrieved in the 332–358 nm wavelength window to avoid interference from O₃ absorption bands below 320 nm. For O₄ and NO₂ DCSD retrievals 350–386 nm and 415–440 nm wavelength windows were used. Details of the cross-sections used and other settings for DOAS analysis are



presented in Table 3. Examples of the fits for O₄, HCHO and NO₂ are shown in Figs. 3(a), 3(b) and 3(c) respectively.

Boundary layer volume mixing ratios for HCHO and NO₂ were calculated from the corresponding trace gas DSCDs using the O₄ DSCDs to calculate the path lengths. Observations with elevation angle of three degrees or less were taken into account to make sure that the corresponding path lengths were close to the elevation of the instrument. Only scans with SZA less than 75° were taken into account. Vertical distribution of O₄ is inversely proportional to the atmospheric pressure. Hence O₄ DSCDs can be used as proxies for the average effective path lengths of measured

Table 3. DOAS analysis settings details.

Parameter	sources	species		
		O ₄	HCHO	NO ₂
Fitting interval		350–386 nm	332–358 nm	415–440 nm
Polynomial degree		3 rd order	3 rd order	3 rd order
Intensity offset		constant	constant	constant
Zenith reference	Zenith from the scan	✓	✓	✓
O ₄	293 K, Thalman and Volkamer (2013)	✓	✓	✓
O ₃	223 K, Bogumil <i>et al.</i> (2003)	✓	✓	✓
	243 K (orthogonalized to O ₃ at 223 K), Bogumil <i>et al.</i> (2003)	✓	✓	✓
NO ₂	294 K, Vandaele <i>et al.</i> (1998)	✓	✓	✓
	220 K (orthogonalized to NO ₂ at 294 K), Vandaele <i>et al.</i> (1998)	✓	✓	✓
HCHO	298 K, Meller and Moortgat (2000)		✓	
CHOCHO				✓
HONO	298 K, Stutz <i>et al.</i> (2000)	✓	✓	
H ₂ O				✓
Ring	Ring spectra, Chance and Kurucz (2010)	✓	✓	✓
	Secondary Ring spectra, Wagner <i>et al.</i> (2009)	✓	✓	✓

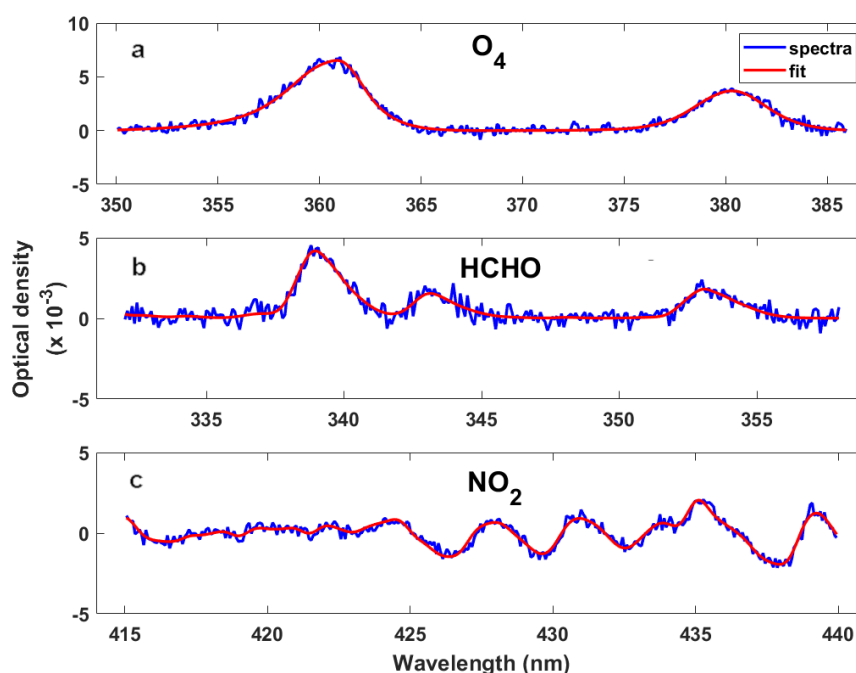
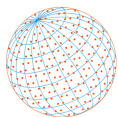


Fig. 3. DOAS fits for O₄, HCHO and NO₂. (a) O₄: 16-May-2018 09:58 hr; SZA: 27.94°; Elevation angle: 1.0°; DSCD: 1.55×10^{43} molecules² cm⁻⁵; RMS: 3.03×10^{-4} . (b) HCHO: 16-May-2018 15:09 hr; SZA: 45.75°; Elevation angle: 1.0°; DSCD: 7.54×10^{16} molecules cm⁻²; RMS: 3.86×10^{-4} . (c) NO₂: 16-May-2018 13:57 hr; SZA: 28.62°; Elevation angle: 1.0°; DSCD: 1.28×10^{16} molecules cm⁻²; RMS: 2.60×10^{-4} .



photons in the boundary layer. Standard atmospheric temperature, pressure, O_4 concentration profiles and measured O_4 DSCDs were used for the calculation of the path length. The O_4 DSCDs were divided by mean O_4 extinction coefficient from surface to 200 m above the instrument level to obtain the path lengths. A wavelength correction was applied to the path length while calculating the NO_2 mixing ratio as spectral windows for O_4 and NO_2 analysis are different. The trace gas mixing ratios were then obtained by dividing the trace gas DSCDs with corresponding path lengths. This methodology was used by other groups in the past (Sinreich *et al.*, 2010; Mahajan *et al.*, 2012).

In addition to ground based observations, satellite observations of vertical column densities (VCDs) were used to study the spatial distribution of trace gases and identify potential source regions which can affect the HCHO and NO_2 mixing ratios at HACPL site. We used monthly averaged trace gas VCDs for the month of May 2018, as measured by the OMI satellite (<http://doi.org/10.18758/71021031>; <http://doi.org/10.21944/qa4ecv-no2-omi-v1.1>). The spatial resolution used for the trace gases was $0.125^\circ \times 0.125^\circ$. The overpass time for OMI over India is 13:45 local time, and hence the satellite retrieved observations will not be representative of sources throughout the day, but should however help identify any large sources in the region.

2.4 Aerosol Optical Depth (AOD) Measurements

AOD measurements were conducted using a sun-sky auto tracking multispectral sun photometer (model: CE 318-M). It measures sun and sky radiance in order to derive the total column water vapor and aerosol properties using a combination of spectral filters and azimuth/zenith viewing. The sun photometer uses different filters to measure solar radiance at 405, 440, 500, 670, 870, 940, 1020, 1640, and 2263 nm wavelengths. These solar extinction measurements are used to compute the AOD at each wavelength except for the 940 nm channel, which is used to retrieve total column water vapor (in cm). The instrument was set to a program-controlled algorithm that performed a scan and generated a maximum of four AOD values in an hour with an interval of 15 min for different wavelengths. In this study, we have used AOD retrieved at the 405 nm wavelength.

2.5 Back Trajectory Analysis

We used the HYbrid Single-Particle Lagrangian Integrated Trajectory (HYSPLIT) (Draxler and Hess, 1998) model to analyse back-trajectories for air parcels sampled at the site. 5 day back trajectories of air masses reaching the HACPL site with 1-hour resolution were calculated using GDAS ($1^\circ \times 1^\circ$) data. Air mass back trajectories reaching at HACPL site during the campaign are shown in Figs. 1(e) and 1(f) (zoomed in version). Synoptic winds at HACPL site were found to be westerly and north-westerly.

3 RESULTS

Time series for the various meteorological parameters measured during the campaign are shown in Fig. 2. The left column shows the temperature (Fig. 2(a)), rainfall (Fig. 2(c)) and wind speed (Fig. 2(e)) and the right column shows the relative humidity (Fig. 2(b)), wind direction (Fig. 2(d)) and boundary layer height (Fig. 2(f)) at the HACPL site. The average temperature was 24.8°C with minimum and maximum temperatures being 18.6°C and 32.6°C , respectively. The average relative humidity was 55.4 % with minimum and maximum relative humidity of 5.6 % and 99.6 %. The average wind speed was 2.6 m s^{-1} with minimum and maximum wind speed of 0.16 m s^{-1} and 11.9 m s^{-1} . Between 10:00–18:00 hrs, the predominant local wind direction was westerly to north-westerly. Rainfall was reported during two days, 17th May, 2018 (5 pm–11 pm) and 25th May, 2018 (1 pm–1.30 pm), reaching a highest precipitation rate of 0.05 mm hr^{-1} . These observations show that the meteorological conditions were similar throughout the entire measurement period and did not contribute heavily to the variations in the trace gases.

During night time, the boundary layer is below the HACPL site elevation and is hence observed as zero in the MWR data. It gradually rises above the observation site in the morning and typically increases to 1000 m and above from the ground level. On most of the days (32 days out of a total 33 days of observation), the boundary layer height evolved to above the HACPL site after ~8 am in the morning. It stays above the measurements site location until about 7 pm, after which the MWR shows a boundary layer height of zero (Fig. 2).

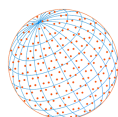


Fig. 4(a) shows the time series of O₄ DSCDs from the present study. Zoomed in view of the daily variation from a typical day during the campaign (5th May, 2018) is presented in Fig. 4(b). Every day, the O₄ DSCD profile showed a skewed 'W' shape with three maxima (Fig. 4(b)). The first maximum occurs in the early morning, second during noon, while the third maximum occurs late in the afternoon. Among these three maxima, the morning maximum was the highest. The presence of three maxima indicates an increasing aerosol loading in the afternoon, which results in a difference from the usual 'U' profile in clean environments. For each scan cycle, lower elevation angles had higher DSCDs compared to the corresponding higher elevation angles. DSCDs elevation angle 3° or lower were used to identify potential days with cloud, dust plumes or any other atmospheric disturbances and corresponding spectra were discarded while calculating mixing ratios for HCHO and NO₂. The average RMS, detection limit and DSCD error for O₄ DSCDs were 4×10^{-4} i.e., 9.3×10^{41} molecule² cm⁻⁵ and 2.2×10^{41} molecule² cm⁻⁵, respectively at the 1° elevation angle. Average O₄ DSCD at the 1° elevation angle was 1.74×10^{43} molecule² cm⁻⁵ with a maximum observed DSCD of 4.4×10^{43} molecule² cm⁻⁵ (Fig. 4(a)). The O₄ DSCDs were then used to estimate the path length and hence the trace gas mixing ratios, as described earlier. Only O₄ DSCDs which passed an RMS filter (RMS < 1e-3), and SZA filter (SZA < 75°) and were free of clouds were used for the calculation of the mixing ratios. The cloud filtering was based on the ratio of radiances at 320 nm and 440 nm (Gielen *et al.*, 2014; Wagner *et al.*, 2014).

The average RMS, detection limit and DSCD error for HCHO DSCDs were 4.4×10^{-4} , 3.45×10^{15} molecules cm⁻² and 2.6×10^{15} molecules cm⁻² respectively at the 1° elevation angle. The average observed HCHO DSCD at 1° elevation angle was 3.5×10^{16} molecules cm⁻², with a maximum DSCD of 8.7×10^{16} molecules cm⁻² (Fig. 4(c)). Elevation angles of 3° and lower accounted for the contribution HCHO near the surface (e.g., Wagner *et al.*, 2004) and were used to calculate the mixing ratios. The resulting time series for HCHO mixing ratios is shown in Fig. 5(a). The average HCHO mixing ratio was 1.6 ± 0.61 ppb (range of 0.16 ppb to 4.8 ppb). The average detection limit for HCHO was 0.3 ppb.

Out of a total of 33 days of observations, after filtering data for meteorological anomalies (e.g., rain) or instrumental issues, HCHO mixing ratios were calculated for 30 days. Out of those 30 days, on 20 days the data was available before 7 am. Out of these 20 days, on 17 days the HCHO mixing ratios either remained constant or slightly decreased over the period of 7–9 am.

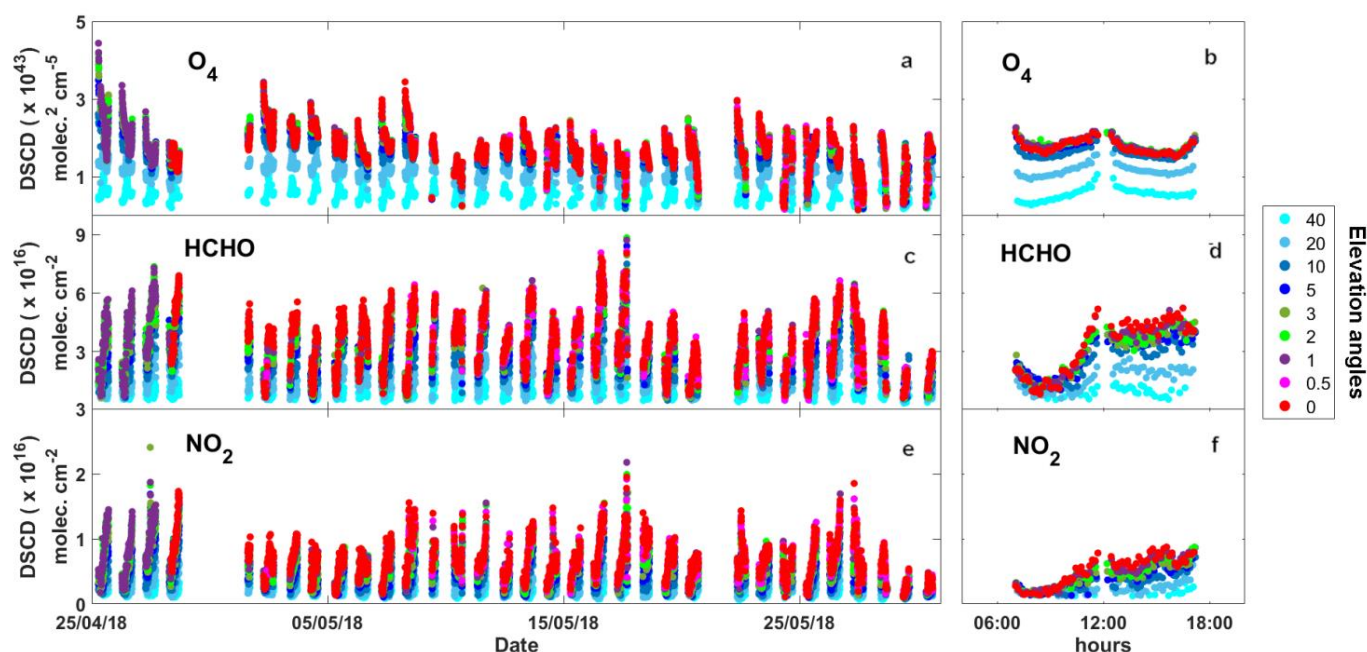


Fig. 4. Timeseries of Differential Slant Column Densities (DSCDs) of (a) O₄, (c) HCHO and (e) NO₂ at the HACPL measurement site. Zoomed in view of DSCDs on 5th May, 2018 are shown in (b) O₄, (d) HCHO and (f) NO₂. Different colors represent measurements at different viewing elevation angles. Measurements of spectra at 0° and 0.5° elevation angles were started on 28th April 2018 with the other angles measured throughout the campaign.

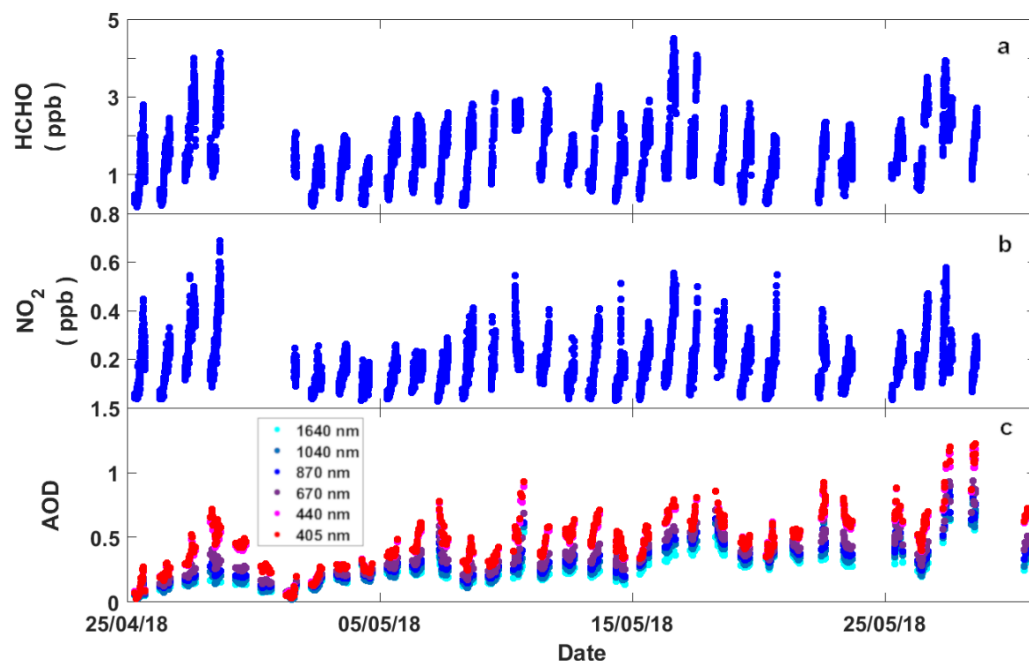
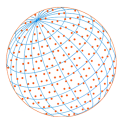


Fig. 5. Time series for HCHO and NO₂ mixing ratios and AOD at six different wavelengths during the campaign at the HACPL site. The panel (a) shows the HCHO mixing ratios; the panel (b) shows the NO₂ mixing ratios; and the panel (c) shows the AOD at different wavelengths.

On the other three days, the HCHO mixing ratio increased over the period of 7–9 am. After 9 am there is an increase in the mixing ratios for all the days. For 23 days out of a total 30 days, mixing ratios were available for 5 pm or later. Out of those 23 days, on 13 days HCHO started decreasing around 3–4 pm. And on three days the decrease in mixing ratios were found later in the day. The diurnal plot of campaign averaged HCHO is shown in Fig. 6(a). The lowest average HCHO mixing ratio was found around 6 am. The mixing ratios remain near constant between 6–9 am after which then increase until 3 pm in the afternoon, reaching a maximum and then decrease steadily.

Fig. 7(a) shows the satellite (OMI) derived spatial distribution of HCHO over India and Fig. 7(b) shows the spatial distribution of HCHO around the HACPL site during May, 2018. We have chosen a 1° × 1° region around the HACPL site to study the spatial distribution. The highest HCHO VCDs were 12.23×10^{15} molecules cm⁻². From the satellite data, we can see that the distribution of HCHO around the site has no distinct emission hotspot.

The average RMS, detection limit and DSCD error for NO₂ DSCDs were 3.1×10^{-4} i.e., 6.72×10^{14} molecules cm⁻² and 3.1×10^{14} at the 1° elevation angle. Average detected NO₂ DSCD at the 1° elevation angle was 6.73×10^{15} molecules cm⁻² with a maximum DSCD of 2.18×10^{16} molecules cm⁻² (Fig. 4(e)). The resulting time series for NO₂ mixing ratios is shown in Fig. 5(b). The average NO₂ mixing ratio was 0.19 ± 0.06 ppb (range of 0.03 ppb to 0.69 ppb). The average detection limit for NO₂ was 0.04 ppb.

For 9 days the NO₂ mixing ratios either decreased or remained constant over the period between 7–9 am. On the other 11 days, the NO₂ mixing ratios increased between 7–9 am. After 9 am there is a steady increase in the NO₂ on all days. On 23 days, data was available for 5 pm or later. Out of those 23 days, on 11 days NO₂ started decreasing around 3–4 pm. A plot showing the diurnal trend of the averaged NO₂ mixing ratios during campaign is presented in Fig. 6(b). The lowest NO₂ mixing ratio was observed around 6 am. Unlike HCHO, NO₂ increases throughout the day reaching maximum at 5 pm.

Figs. 7(c) and 7(d) show the OMI satellite observed spatial distribution of NO₂ VCDs over India and around the HACPL site. The average NO₂ VCDs over the HACPL site was $\sim 1.53 \times 10^{15}$ molecules cm⁻². In the north-east direction, the highest NO₂ VCDs was 2.82×10^{15} molecules cm⁻² was observed and coincided with city of Pune. Regions within the immediate vicinity of the HACPL site displayed low NO₂ VCDs with a homogeneous spatial distribution. Emissions from Pune city are a potential

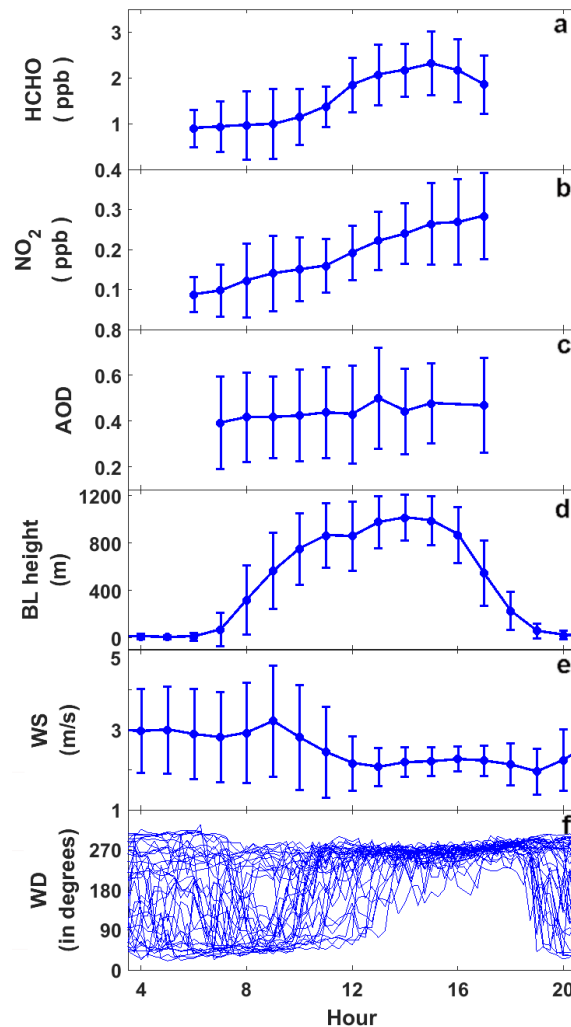
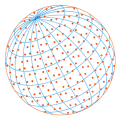


Fig. 6. Averaged diurnal variation in (a) HCHO and (b) NO₂ mixing ratios, (c) AOD at 405 nm, (d) BL height and (e) wind speed during the campaign at HACPL. The error bars represent the standard deviations. Panel (f) shows the daily diurnal variation of wind direction during the campaign period at HACPL site.

source of NO₂ that was observed at the HACPL site. We used the HYbrid Single-Particle Lagrangian Integrated Trajectory (HYSPLIT) model to calculate back-trajectories for air parcels sampled at the site and found that none of them came from the north-east. Back trajectories were sampled at HACPL site showed westerly to north-westerly synoptic winds (Figs. 1(e) and 1(f)). All the back-trajectories observed during this campaign were from north-west direction and hence NO₂ emissions from the Pune City can be ruled out as a potential source for NO₂.

Although AOD at all the six wavelengths showed a similar diurnal variation, AOD at 405 nm showed largest variation throughout the day (Fig. 5(c)). Due to Mie scattering, photons are scattered by particles which have diameters equivalent to or larger than the wavelength of the photon. More scattering will result in higher AOD. The high variation in AOD at 405 nm indicates presence of smaller particles. Hence, we will discuss AOD in terms of AOD at 405 nm. A diurnal plot of the campaign averaged AOD at 405 nm is shown in Fig. 6(c). The averaged AOD at 405 nm steadily increases throughout the day reaching maximum at in the late afternoon, although the variation is not significant when averaged over the whole campaign.

4 DISCUSSIONS

In the MAX-DOAS technique, scattered solar radiation is recorded and processed to find

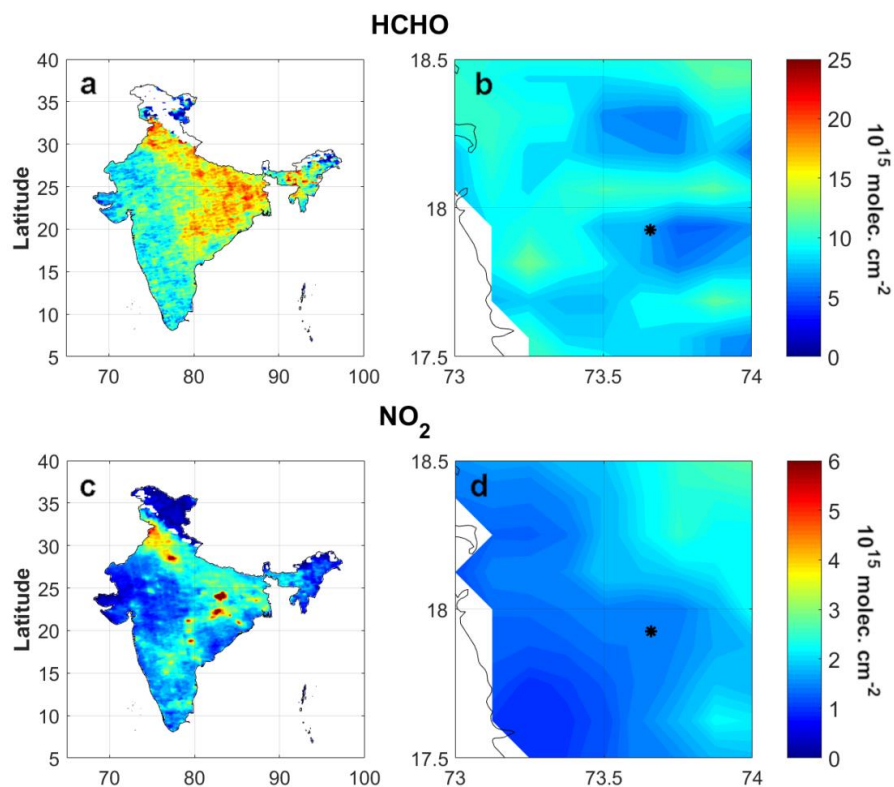
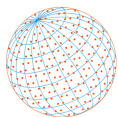
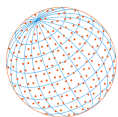


Fig. 7. Satellite (OMI) retrieved vertical columns of HCHO and NO₂ for the month of May, 2018. The top row shows the HCHO vertical column distribution over (a) India and over (b) the HACPL site. The bottom row shows NO₂ vertical column distribution over (s) India and over (d) the HACPL site. The '*' sign represents the location of measurement site.

concentrations of absorber species present in the atmosphere using laboratory measured absorption cross-sections. Measurements at lower elevation angles are more sensitive towards lower tropospheric absorbers as photons travel longer path lengths through the lower troposphere as compared to higher elevation angles. O₄ absorption is proportional to the square of the oxygen pressure, hence higher O₄ DSCDs are expected at lower elevation angles unless the photons undergo multiple scattering. Compared to the observations in the rural IGP region during the Asian Summer Monsoon (ASM) period (Biswas *et al.*, 2019), the O₄ DSCDs from elevation angles less than 3° were higher compared to the 5–7°. This indicates low levels of aerosols and clouds as compared to the rural IGP region. This is expected considering that the HACPL is a high altitude site, with fewer direct sources of natural and anthropogenic aerosols as compared to the heavily populated IGP.

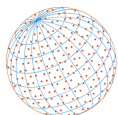
The diurnal variation in NO₂ mixing ratios at rural sites usually follows a 'U' shaped pattern due to daytime destruction of NO₂ by photochemistry. NO₂ photochemically dissociates to form NO and reactive oxygen (O(³P)). O(³P) then reacts with O₂ to form O₃ (Atkinson, 2000 and references therein). Recently, Biswas *et al.* (2019) observed this expected diurnal variation of NO₂ at a rural site in the IGP region. The same diurnal profile has been reported by Renuka *et al.* (2014) and Reddy *et al.* (2012) from two different rural sites in southern India. Li *et al.* (2013) also reported a similar diurnal variation at a rural site in Southern China. Considering the lack of a strong emission point close to the measurement site (Fig. 7(d)), one would expect a similar 'U' shape in NO₂ at the HACPL site. However, the observed diurnal pattern of NO₂ is different compared to these other rural sites. As seen in Fig. 6(b), NO₂ mixing ratios increase (from 0.09 ppb to 0.28 ppb) throughout the day from 6 am to 5 pm. Although the NO₂ mixing ratios started decreasing after 3–4 pm on some days (11 days), the campaign average diurnal variation showed an increasing trend till 5 pm. Additionally, NO₂ decreased or remained constant between 7–9 am on 9 days. These features indicate that a different mechanism determined the diurnal variation instead of the expected control by photochemistry.



In the case of HCHO, Biswas *et al.* (2019) reported a diurnal pattern with an early morning increase until 11 am in the morning due to production from photochemical oxidation of VOCs in the rural IGP. Emission of biogenic VOCs shows effects of temperature control. During the daytime, the emissions of biogenic VOCs increase but around noon, the loss processes start to dominate. HCHO converts to HCO radical by photodissociation or by oxidation by hydroxyl radicals (OH) finally oxidized to CO₂. After 11 am, photochemical destruction of HCHO is observed to dominate and mixing ratios start to decrease. By the end of the day, the HCHO values are similar to the early morning in the IGP (1.5 ± 1 ppb). In the Borneo rainforest, Macdonald *et al.* (2012) studied the diurnal variation in HCHO mixing ratios and reported that the values increased during the morning, reaching a peak around 1–2 pm and then decreased sharply. In this case, since there were much larger sources of VOCs, the peak in HCHO was later than in the IGP (Biswas *et al.*, 2019). Biesenthal *et al.* (1998) and Wang *et al.* (2010) have also reported a similar diurnal trend from Eastern Canada and Eastern China respectively. From Fig. 6(a), we can see that the averaged HCHO mixing ratios at HACPL site remained near constant for the period between 7–9 am. From 9 am to 3 pm the HCHO mixing ratio increased reaching a maximum (from 1 ppb to 2.3 ppb) and then decreased slightly (from 2.3 ppb to 1.9 ppb). At HACPL, the peak was observed much later in the day compared to the other observations from around the world in rural environments and the peak was not as pronounced as expected due to a smaller decrease in the HCHO mixing ratios. Indeed, the HCHO mixing ratios an increasing average diurnal pattern during daytime and did not show a typical photochemistry dominated profile.

Similar diurnal variations in both the trace gases indicates that the HCHO and NO₂ mixing ratios were controlled by a common factor rather than photochemistry, which would have led to very distinct profiles in both the species. We hypothesize that the evolution of the boundary layer is a major factor behind the observed diurnal pattern in the HCHO and NO₂ mixing ratios. The average diurnal variation in the boundary layer height is shown in Fig. 6(d). During the early morning (6–8 am) the boundary layer is below the HACPL site (as evidenced by the boundary layer height observations, Fig. 6(d)). During this period, the MAX-DOAS mainly samples free tropospheric air, which contains lower amounts of the trace gases as the main emissions are within the boundary layer at the base of the mountain. Therefore the lowest average mixing ratios for both NO₂ and HCHO were found at 6 am (Figs. 6(a) and 6(b)). Between 8–9 am (on some days even later) the boundary layer evolves due to solar heating and rises above the HACPL site. As the boundary layer increases above the measurement point, the MAX-DOAS samples trace gases within the boundary layer. As the day progresses, the boundary layer height and the turbulent kinetic energy increases, leading to further mixing of gases within the boundary layer. Emissions from nearby villages and towns from the mountain base also increase during daytime and get well mixed within the boundary layer. HCHO mixing ratios show a steep increase from 9 am to 10 am and then continue increasing till 3 pm. NO₂ mixing ratio follows an increasing trend from 6 am in the morning to 5 pm in the evening. In the afternoon, the boundary layer height starts decreasing after 5 pm. By 3 pm solar radiation also shows a decrease, hence the photochemical production of HCHO from VOCs also decreases resulting in decreased HCHO mixing ratios. However, in the case of NO₂, the photochemical loss decreases due to lower solar radiation and hence the mixing ratios continue increasing until the end of the day.

Considering that the primary sources (both biogenic and anthropogenic) of NO₂ and HCHO are near the surface, it is expected that the observed diurnal variation in both the trace gases would reflect the variation in the boundary layer. Another parameter that can be used as tracer for boundary layer evolution is the presence of aerosols and hence we analyzed the time series and diurnal variation of AOD at 405 nm at HACPL. AOD is the measure of extinction of solar radiation by aerosol; hence it can be used as proxy for aerosol concentration. Here we assume that a large portion of the aerosols is trapped within the boundary layer. If evolution of the boundary layer is the main reason for the observed trend in HCHO and NO₂ mixing ratios, we should expect a similar trend in the AOD. The campaign averaged diurnal plot of AOD at 405 nm (Fig. 6(c)) shows an increase from 7 am in the morning until the evening confirming the hypothesis, however, the standard deviation is large. During the pre-monsoon period, aerosol loading increases over Indian sub-continent due to the lack of rainfall (Bollasina *et al.*, 2008; Gautam *et al.*, 2009). The increase in AOD at 405 nm during pre-monsoon period is thus a result of increasing aerosol loading, which can be seen in Fig. 5(c). To study the day to day variability we removed the background increasing



trend which was due to this large-scale increase in aerosols over the Indian sub-continent (pre-monsoon aerosols). The daily averaged NO_2 and HCHO mixing ratios did not show any increasing trend during the campaign period, unlike the AOD. As sources of trace gases and aerosols change with time within a day, correlating trace gas and AOD data for shorter timescale will be erroneous. Hence, we studied the correlation between daily averaged de-trended AOD at 405 nm and daily averaged mixing ratios of HCHO and NO_2 (Figs. 8(a) and 8(b)). A positive correlation was observed between the AOD and the HCHO ($R = 0.58$, $P < 0.01$) and NO_2 ($R = 0.44$, $P < 0.01$) mixing ratios. Scatter plots for the daily averaged AOD against the daily average trace gas mixing ratios showed that higher AOD coincide with the days where elevated trace gas mixing ratios were observed (Figs. 8(c) and 8(d)). A similar result was obtained using the BL height to understand the evolution the trace gas mixing ratios, which showed that higher BL height were coincident with elevated trace gas mixing ratios, with high mixing ratios observed only when the BL height was larger (Figs. 8(e) and 8(f)). These re-confirm our initial hypothesis that the boundary layer evolution contributes to the HCHO and NO_2 observations at the HACPL measurement site.

In a similar study, Schreier *et al.* (2016) have reported free tropospheric NO_2 and HCHO from two high altitude sites in Zugspitze, Germany and Pico Espejo, Venezuela. They reported an increasing diurnal trend in NO_2 mixing ratios from 7 am to 2 pm followed by a decrease in

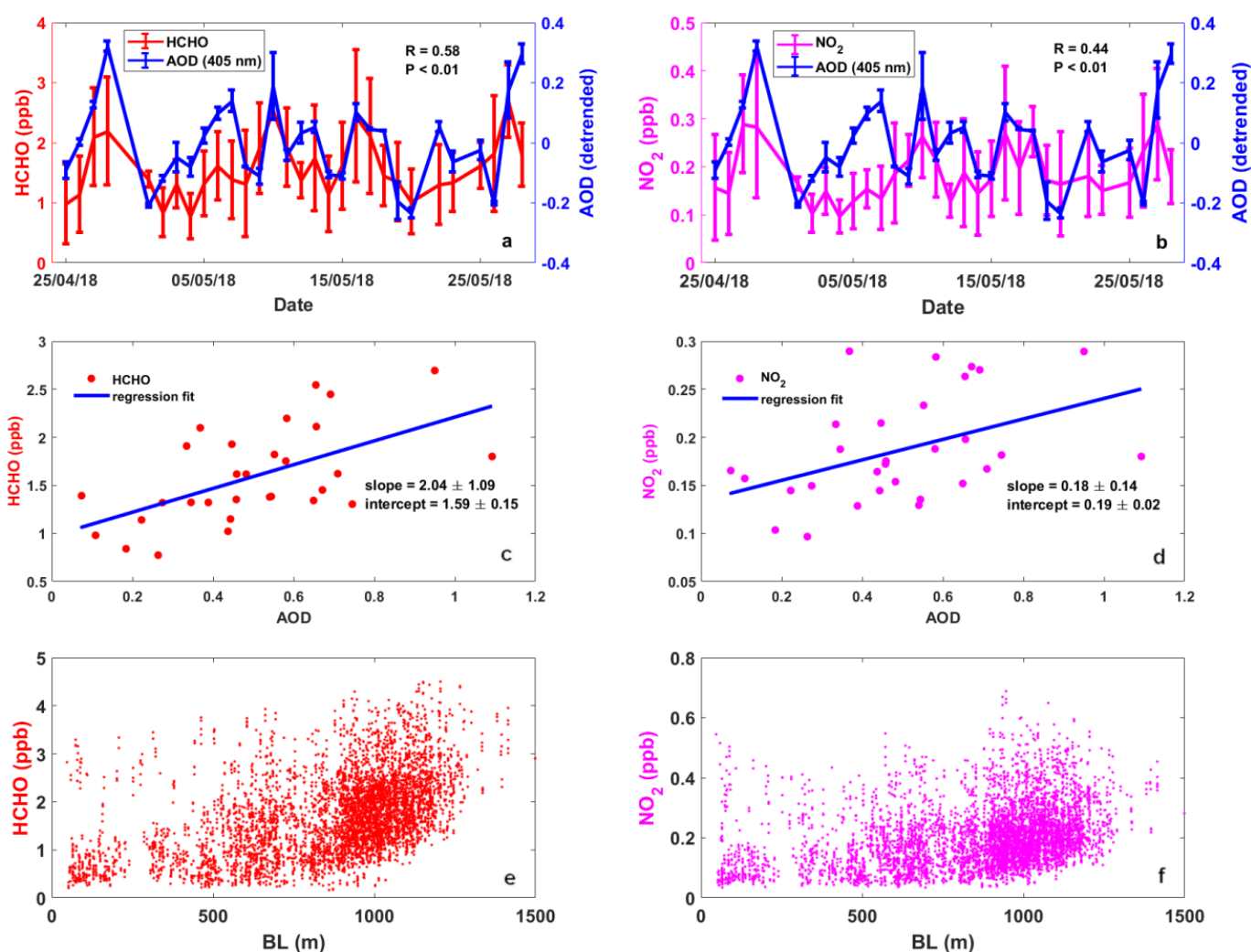
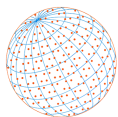


Fig. 8. Correlation between (a) daily average de-trended AOD at 405 nm and the daily averaged HCHO and (b) daily average de-trended AOD at 405 nm and the daily averaged NO_2 plots as observed through the campaign. Correlation coefficient, R and P value from the regression analysis are shown in the plot. Regression fit for (c) daily average AOD at 405 nm and the daily averaged HCHO and (d) daily average AOD at 405 nm and the daily averaged NO_2 with slope and intercepts information. Scatter plot of (e) BL height vs. HCHO and (f) BL height vs. NO_2 .



Zugspitze, Germany. They also reported a decreasing diurnal HCHO mixing ratio during 7–10 am followed by an increase until 4 pm. They found a statistically significant linear relationship between monthly averaged AOD and NO₂, leading to a conclusion that AOD and NO₂ were related to pollution in the experimental site. This was corroborated by a linear relationship between monthly averaged fire radiative power and both the trace gas mixing ratios, suggesting biomass burning sources. However, they did not comment on the observed diurnal variation of trace gases, which was similar to the observations reported in this study and show indications of boundary layer dynamics playing a role. Gil-Ojeda *et al.* (2015) also reported free tropospheric NO₂ observations from Izana Mountain Spain. The diurnal profile reported in that study for 8th May 2013 showed an increase in NO₂ mixing ratios till from the morning until ~12 pm, reaching a plateau followed by a decrease in the late afternoon. This observation also follows the current study, and is indicative of boundary layer dynamics affecting trace gas observations at those high altitude sites. Naja *et al.* (2003) reported observations of O₃ and oxides nitrogen (NO + NO_x) from high altitude site at Mt. Abu in central-west India. Analyzing the trace gas observations and correlating the results with similar work from around the world they have concluded that the boundary layer height evolution was one the main contributing factor of observed diurnal variation trace gas. Sarangi *et al.* (2013) have reported simultaneous measurements of O₃, carbon monoxide (CO) and oxides nitrogen (NO_y) at a high-altitude Himalayan site in Nainital, India. Comparing the observed diurnal variation with other global sites, they have concluded that the dynamical processes (e.g., the boundary layer evolution, mountain winds along with the transport) and en route photochemistry have larger effect compared to in-situ photochemistry on the trace gas concentration at Nainital. Both Naja *et al.* (2003) and Sarangi *et al.* (2013) neither reported NO₂ and HCHO observations nor the diurnal variation of their concentrations. Although both Naja *et al.* (2003) and Sarangi *et al.* (2013) reported boundary layer evolution as one of the main controlling factor of trace gas concentration at Mt. Abu and Nainital, they have not reported any study using boundary layer observation data. In the present work we have used boundary layer observations, AOD observations and satellite observations along with the trace gas observations to show the clear effect of the boundary layer on both the trace gases.

We selected one typical day when the NO₂ and HCHO mixing ratios and AOD at 405 nm followed similar trends (27th April, 2018; Fig. 9). It can be seen that the boundary layer rises above the HACPL site at 8 am and reaches a plateau at ~1000 m above the measurement site around 9:30 am. The maximum height observed on this day is about ~1500 m above ground around at 3 pm. After 3 pm the boundary layer height starts decreasing and by 7 pm the boundary layer falls below the HACPL site. The HCHO mixing ratios start increasing (from 0.84 ppb) at 7 am in the morning and reach a maximum (~4 ppb) at around 3:30 pm. After reaching the peak, HCHO mixing ratios start decreasing gradually until 5 pm. NO₂ mixing ratios also follow a similar trend. The NO₂ mixing ratios start increasing (from 0.12 ppb) at 7 am in the morning and after a brief dip around 9 am, keep increasing (0.5 ppb) till 3:30 pm. There is a sudden increase (0.54 ppb) in NO₂ mixing ratio around 11:30 am, which is probably due to local sources or biomass burning from the neighboring villages. After 3:30 pm the NO₂ mixing ratios start decreasing until 5 pm. There was an early morning data gap in AOD observation. But the AOD at 405 nm starts increasing from ~8:30 am in the morning until 3:30 pm (from 0.3 to 0.42). This diurnal pattern follows our conclusion that boundary layer dynamics affects the trace gas mixing ratios and the measured AOD.

Additionally, we selected another day during campaign when the diurnal variation in HCHO and NO₂ mixing ratios match the diurnal variation in boundary layer height but the AOD diurnal variation does not (23rd May, 2018; Fig. 10). On this day, the boundary layer rises above the HACPL site at ~10 am which is late compared to the other days during campaign period. After that the boundary layer height reaches a plateau at ~1000 m above the HACPL site around 1 pm. After 4 pm the boundary layer height starts decreasing and by 7 pm it falls below the HACPL site. The HCHO mixing ratios start decreasing (from 1.33 ppb) at 7 am in the morning reaching a minimum (0.45 ppb) at around 10 am. This can be explained as boundary layer height was below the HACPL site till 10 am; hence VOCs and OVOCs from within the boundary layer are not sampled by the MAX-DOAS. Indeed, during the same period the HCHO present in the free troposphere is being depleted due to photodissociation and the sources are not contributing and hence a decrease is expected. After 10 am, when the boundary layer evolves, the HCHO mixing ratios start increasing and reach a plateau (2.3 ppb) by ~2 pm. After 4 pm the HCHO mixing ratios start decreasing rapidly,

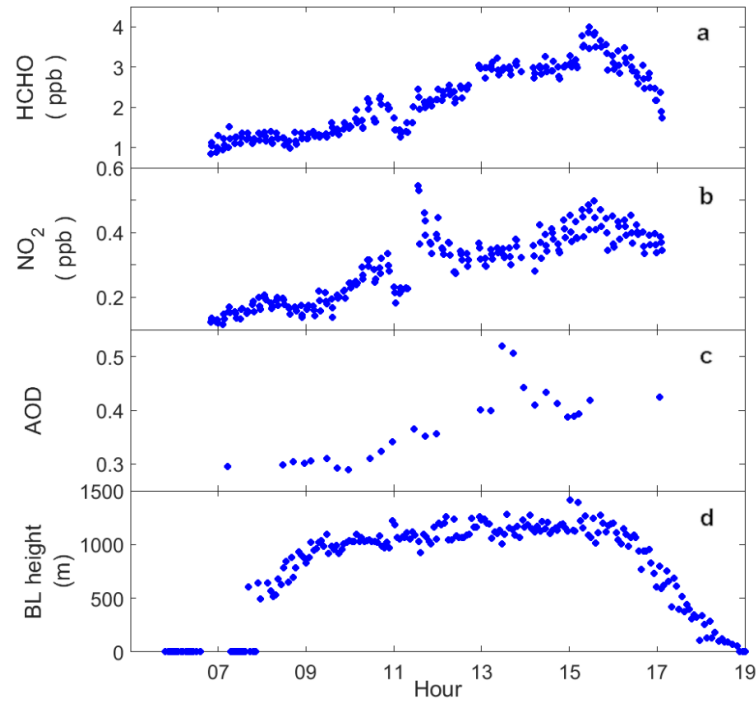
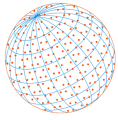


Fig. 9. (a) HCHO, (b) NO₂ mixing ratios, (c) AOD at 405 nm and (d) boundary layer height on 27th April 2018.

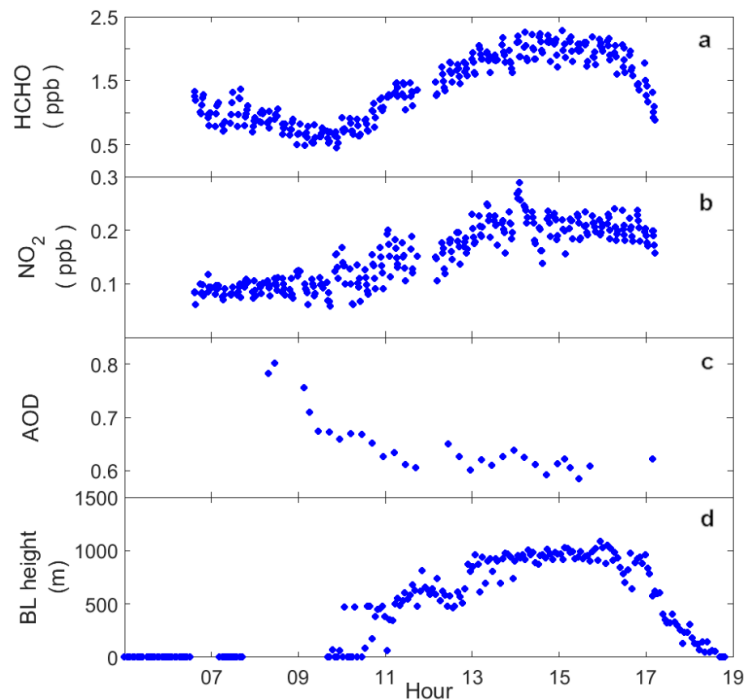
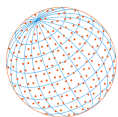


Fig. 10. (a) HCHO, (b) NO₂ mixing ratios, (c) AOD at 405 nm and (d) boundary layer height on 23rd May 2018.

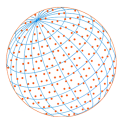
as expected due to the decrease in the boundary layer. NO₂ mixing ratios remained steady (~0.1 ppb) during the period 7–10 am showing that no new sources were contributing to the NO₂. After 10 am the NO₂ mixing ratios start to increase reaching a plateau (~0.2 ppb) around 2 pm followed by a decrease around 5 pm, as expected due to the boundary layer evolution on this day. In contrary to the previous example of 27th April, 2018 (Fig. 9), the AOD at 405 nm starts



decreasing rapidly at around 8 am until 11.30 am (from 0.8 to 0.6). After that it remained steady. From Figs. 5 and 10, we can see that on the morning of 23rd May, 2018, the AOD at 405 nm was much higher than the average AOD through the month (0.8 compared to 0.4). This was probably due to an aerosol plume which arrived at the HACPL site on 23rd May, 2018. To check this, we looked at the 5-day back trajectories for the early morning on this day, which showed that the air masses arriving at the measurement site had originated towards the west of India close the Middle East and had spent most of their time close to the surface. This is contrary to most of the other days, which did not have a strong influence of the boundary layer in their air-masses and hence had much lower aerosol loading. Later in the day, the AOD decreased and reached the levels of AOD typically observed at the site due to the removal of aerosols by either transport or deposition and a change in the back-trajectories. Hence, even though the AOD does not follow the typical diurnal profile, it can be concluded that the controlling factor for the trends in the mixing ratios of HCHO and NO₂ was BL evolution and dynamics.

We studied the effect of the locally measured wind direction and wind speed on the trace gas mixing ratios. Fig. 6(e) shows the diurnal variation in the wind speed and Fig. 6(f) shows the daily diurnal variation of wind direction at the HACPL site. From Fig. 6(f) we can see that between 10:00–18:00, the wind was mainly westerly to north-westerly. However, during rest of the day the local wind showed a variation in the directionality. Between 10:00–18:00 the average wind speed was lower compared to other time of the day (Fig. 6(e)). There were a few days when the westerly/north-westerly wind prevailed throughout the day and few days when the easterly/north-easterly wind was observed till late afternoon. However, by late afternoon, on all the days, the local winds were westerly to north-westerly. We identified the days when the local wind direction was westerly to north-westerly before 10:00 hrs, and days when the local wind direction was easterly to north-easterly till late afternoon. When the wind was from the east and north-east direction, higher mixing ratios were observed for both the trace gases. This indicates that the wind from the towns of Panchgani and Wai (which are to the East as mentioned above) resulted in higher trace gas concentration at HACPL. However, it is important to note that the diurnal variation for both the trace gases in all the cases showed an increase in mixing ratios throughout the days, and was not indicative of traffic peaks or of photochemistry domination, but rather controlled by the BL evolution. This indicates that although wind from different directions may affect the absolute mixing ratios, the boundary layer evolution controls the diurnal trend of trace gas mixing ratios at HACPL.

We reach the conclusion that the observed diurnal variation of NO₂ and HCHO at HACPL site is due to the following three reasons. Firstly, from the boundary layer height data it is evident that the boundary layer resides below the HACPL observation site in the early morning (till 7–9 am). Hence the MAX-DOAS observations were sampling air from free troposphere which are mostly independent of the surface emissions and have low trace gas concentrations. This explains the fact that the mixing ratios of both the trace gases were low in the early morning. At these hours, source emission intensities from the base of the mountain or other regions did not affect MAX-DOAS observation at HACPL site. Secondly, after 7–9 am in the morning, the boundary layer height increases due to the heating by solar radiation. Slowly, the boundary layer height rises above the HACPL site and subsequent MAX-DOAS observations start to sample the air within boundary layer which contains emissions from the base of the mountain. As the day progresses, along with increased solar radiation there is better mixing of trace gases emitted from the mountain base throughout the boundary layer due to an increase in the turbulent kinetic mixing. Better mixing helps the emitted trace gases from mountain base to reach the height of MAX-DOAS observations and increase the observed trace gas concentrations. Finally, during the course of the day, the emissions of the anthropogenic trace gases (NO₂ and HCHO) increases due to increase in anthropogenic activities. Meanwhile the biogenic trace gases (HCHO) also increase due to the increased photochemical synthesis from their precursors due to reactive chemistry in the atmosphere in presence of solar radiation. These contribute to sustain the observed increase in NO₂ and HCHO mixing ratios. Later in the afternoon, decrease in the incoming solar radiation causes reduction in the photochemical synthesis of HCHO resulting in a decrease in HCHO in the late afternoon. Whereas the decreased incoming solar radiation causes reduction in photochemical destruction of NO₂ and hence the NO₂ tends to increase till late afternoon. The observed diurnal variation in the trace gas concentration is independent of the source type (anthropogenic or biogenic). This study only rationalizes the



reason behind observed diurnal variation in the trace gas concentration without explicitly identifying their source.

The present work is part of a larger project which aims to understand the geographical distribution of these trace gases over India and find the main drivers of their chemistry in different environments. Here our aim was to study the diurnal variation of the trace gases for the pre-monsoon period to understand the drivers and we achieved that using four different types of observations. This short term observation campaign established the fact that HACPL site is indeed different from other sites in terms of the driving factors for trace gas chemistry, where such observations were conducted around India. In future we plan to study long term observations of these trace gases to better understand the tropospheric chemistry over India.

5 CONCLUSIONS

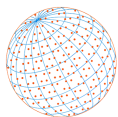
In this study we report observations of HCHO and NO₂ at the HACPL in Mahabaleshwar, a hill station in Western Ghats region of India. We studied the diurnal variation of these two trace gases and discuss the possible reasons behind the observed diurnal variation. The average NO₂ mixing ratio was 0.19 ± 0.06 ppb (range of 0.03 ppb to 0.69 ppb). The NO₂ mixing ratios were found to increase from early in the morning and reached a maximum in the afternoon. This is contradictory to the photochemistry driven NO₂ profile in rural areas where NO₂ mixing ratios show a dip during the daytime. The average HCHO mixing ratio was 1.6 ± 0.61 ppb (range of 0.16 ppb to 4.5 ppb). HCHO was found to increase from early in the morning and reached a maximum at ~3 pm in the afternoon and then showed a small decrease. This is also contradictory to the typical photochemistry driven diurnal HCHO profile, where the mixing ratios reach a peak earlier in the day followed by significant decrease through the afternoon. Additionally, the daily averaged trace gas mixing ratios show a positive correlation with daily averaged AOD ($R = 0.58$, $P < 0.01$ for HCHO and AOD; $R = 0.44$, $P < 0.01$ for NO₂ and AOD). Using observations of the boundary layer height, it is concluded that the observed diurnal variations of NO₂ and HCHO, which have very different photochemistry, show similar diurnal profile due to the evolution of boundary layer at the HACPL site. The boundary layer resides below the site during the morning and rise above the site around 8 am in the morning until about 7 pm after which the measurement site is again above the boundary layer. Observations show that trace gas mixing ratios start increasing after the boundary layer is above the HACPL site and decrease as the boundary layer height decreases. We concluded that during the morning the MAX-DOAS samples air in free troposphere which does not contain emissions from neighboring villages at the base of the mountain. As the boundary layer rises above the HACPL site, the MAX-DOAS samples the well mixed air which contains emissions from the mountain base. This study, in addition to reporting the first simultaneous observations NO₂ and HCHO in the Western Ghats region of India also explains the dominant effects controlling the diurnal evolution of both the species using boundary layer observations, AOD observations along with the trace gas observations.

ACKNOWLEDGEMENTS

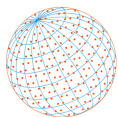
The Indian Institute of Tropical Meteorology is funded by the Ministry of Earth Sciences, Government of India. We thank the High Altitude Cloud Physics Laboratory (HACPL) for support during the measurement period.

REFERENCES

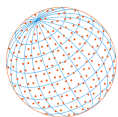
- Atkinson, R. (2000). Atmospheric chemistry of VOCs and NO_x. *Atmos. Environ.* 34, 2063–2101. [https://doi.org/10.1016/S1352-2310\(99\)00460-4](https://doi.org/10.1016/S1352-2310(99)00460-4)
- Biesenhal, T.A., Bottenheim, J.W., Shepson, P.B., Li, S.M., Brickell, P.C. (1998). The chemistry of biogenic hydrocarbons at a rural site in eastern Canada. *J. Geophys. Res.* 103, 25487–25498. <https://doi.org/10.1029/98JD01848>
- Biswas, M.S., Ghude, S., Gurnale, D., Prabhakaran, T., Mahajan, A.S. (2019). Simultaneous



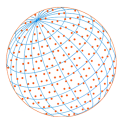
- observations of nitrogen dioxide, formaldehyde and ozone in the Indo-Gangetic Plain. *Aerosol Air Qual. Res.* 19, 1749–1764. <https://doi.org/10.4209/aaqr.2018.12.0484>
- Bogumil, K., Orphal, J., Homann, T., Voigt, S., Spietz, P., Fleischmann, O.C., Vogel, A., Hartmann, M., Kromminga, H., Bovensmann, H., Frerick, J., Burrows, J.P. (2003). Measurements of molecular absorption spectra with the SCIAMACHY pre-flight model: Instrument characterization and reference data for atmospheric remote-sensing in the 230–2380 nm region. *J. Photochem. Photobiol., A* 157, 167–184. [https://doi.org/10.1016/S1010-6030\(03\)00062-5](https://doi.org/10.1016/S1010-6030(03)00062-5)
- Bollasina, M., Nigam, S., Lau, K.M. (2008). Absorbing aerosols and summer monsoon evolution over South Asia: An observational portrayal. *J. Clim.* 21, 3221–3239. <https://doi.org/10.1175/2007JCLI2094.1>
- Burnett, R.T., Stieb, D., Brook, J.R., Cakmak, S., Dales, R., Raizenne, M., Vincent, R., Dann, T. (2004). Associations between short-term changes in nitrogen dioxide and mortality in Canadian cities. *Arch. Environ. Health* 59, 228–36. <https://doi.org/10.3200/AEOH.59.5.228-236>
- Carrier, P., Hannachi, H., Mouvier, G. (1986). The chemistry of carbonyl compounds in the atmosphere—A review. *Atmos. Environ.* 20, 2079–2099. [https://doi.org/10.1016/0004-6981\(86\)90304-5](https://doi.org/10.1016/0004-6981(86)90304-5)
- Carter, W.P.L., Atkinson, R. (1987). An experimental study of incremental hydrocarbon reactivity. *Environ. Sci. Technol.* 21, 670–679. <https://doi.org/10.1021/es00161a008>
- Chance, K., Kurucz, R.L. (2010). An improved high-resolution solar reference spectrum for earth's atmosphere measurements in the ultraviolet, visible, and near infrared. *J. Quant. Spectrosc. Radiat. Transfer* 111, 1289–1295. <https://doi.org/10.1016/j.jqsrt.2010.01.036>
- Crutzen, B.P.J. (1974). Photochemical reactions initiated by and influencing ozone in unpolluted tropospheric air. *Tellus* 1–2, 47–57. <https://doi.org/10.3402/tellusa.v26i1-2.9736>
- Danckaert, T. (2014). QDOAS Software user manual.
- Draxler, R.R., Hess, G.D. (1998). An Overview of the HYSPLIT_4 Modelling System for Trajectories, Dispersion, and Deposition. *Aust. Meteorol. Mag.* 47, 295–308.
- Dutta, C., Chatterjee, A., Jana, T.K., Mukherjee, A.K., Sen, S. (2010). Contribution from the primary and secondary sources to the atmospheric formaldehyde in Kolkata, India. *Sci. Total Environ.* 408, 4744–4748. <https://doi.org/10.1016/j.scitotenv.2010.01.031>
- Epa, U. (2015). Technical Support Document EPA's 2011 National-scale Air Toxics Assessment, 2011 NATA TSD.
- Finlayson-Pitts, B., Pitts, J.N. (2000). *Chemistry of the upper and lower atmosphere*, 1st ed. Academic Press.
- Fu, T.M., Jacob, D.J., Palmer, P.I., Chance, K., Wang, Y.X., Barletta, B., Blake, D.R., Stanton, J.C., Pilling, M.J. (2007). Space-based formaldehyde measurements as constraints on volatile organic compound emissions in east and south Asia and implications for ozone. *J. Geophys. Res.* 112, D06312. <https://doi.org/10.1029/2006JD007853>
- Gautam, R., Hsu, N.C., Lau, K.M., Tsay, S.C., Kafatos, M. (2009). Enhanced pre-monsoon warming over the Himalayan-Gangetic region from 1979 to 2007. *Geophys. Res. Lett.* 36, L07704. <https://doi.org/10.1029/2009GL037641>
- Gielen, C., Van Roozendaal, M., Hendrick, F., Pinardi, G., Vlemmix, T., De Bock, V., De Backer, H., Fayt, C., Hermans, C., Gillotay, D., Wang, P. (2014). A simple and versatile cloud-screening method for MAX-DOAS retrievals. *Atmos. Meas. Tech.* 7, 3509–3527. <https://doi.org/10.5194/amt-7-3509-2014>
- Gil-Ojeda, M., Navarro-Comas, M., Gómez-Martín, L., Adame, J.A., Saiz-Lopez, A., Cuevas, C.A., González, Y., Puertedura, O., Cuevas, E., Lamarque, J.F., Kinnison, D., Tilmes, S. (2015). NO₂ seasonal evolution in the north subtropical free troposphere. *Atmos. Chem. Phys.* 15, 10567–10579. <https://doi.org/10.5194/acp-15-10567-2015>
- Hak, C., Pundt, I., Trick, S., Kern, C., Platt, U., Dommen, J., Ordóñez, C., Prévôt, A.S.H., Junkermann, W., Astorga-Lloréns, C., Larsen, B.R., Mellqvist, J., Strandberg, A., Yu, Y., Galle, B., Kleffmann, J., Lörzer, J.C., Braathen, G.O., Volkamer, R. (2005). Intercomparison of four different in-situ techniques for ambient formaldehyde measurements in urban air. *Atmos. Chem. Phys.* 5, 2881–2900. <https://doi.org/10.5194/acp-5-2881-2005>
- Herndon, S.C., Jayne, J.T., Zahniser, M.S., Worsnop, D.R., Knighton, B., Alwine, E., Lamb, B.K., Zavale, M., Nelson, D.D., McManus, J.B., Shorter, J.H., Canagaratna, M.R., Onasch, T.B., Kolb, C.E. (2005). Characterization of urban pollutant emission fluxes and ambient concentration



- distributions using a mobile laboratory with rapid response instrumentation. *Faraday Discuss.* 130, 327–339. <https://doi.org/10.1039/B500411J>
- Hönninger, G., von Friedeburg, C., Platt, U. (2004). Multi axis differential optical absorption spectroscopy (MAX-DOAS). *Atmos. Chem. Phys.* 4, 231–254. <https://doi.org/10.5194/acp-4-231-2004>
- Hoque, H.M.S., Irie, H., Damiani, A., Rawat, P., Naja, M. (2018). First simultaneous observations of formaldehyde and glyoxal by MAX-DOAS in the Indo-Gangetic Plain region. *Sola* 14, 159–164. <https://doi.org/10.2151/sola.2018-028>
- Jacob, D.J. (2000). Heterogeneous chemistry and tropospheric ozone. *Atmos. Environ.* 34, 2131–2159. [https://doi.org/10.1016/S1352-2310\(99\)00462-8](https://doi.org/10.1016/S1352-2310(99)00462-8)
- Jaeglé, L., Steinberger, L., Martin, R.V., Chance, K. (2005). Global partitioning of NO_x sources using satellite observations: Relative roles of fossil fuel combustion, biomass burning and soil emissions. *Faraday Discuss.* 130, 407. <https://doi.org/10.1039/b502128f>
- Khare, P., Satsangi, G.S., Kumar, N., Kumari, K.M., Srivastava, S.S. (1997a). HCHO, HCOOH and CH₃COOH in air and rain water at a rural tropical site in North Central India. *Atmos. Environ.* 31, 3867–3875. [https://doi.org/10.1016/S1352-2310\(97\)00263-X](https://doi.org/10.1016/S1352-2310(97)00263-X)
- Khare, P., Satsangi, G.S., Kumar, N., Kumari, K.M., Srivastava, S.S. (1997b). Surface measurements of formaldehyde and formic and acetic acids at a subtropical semiarid site in India. *J. Geophys. Res.* 102, 18997–19005. <https://doi.org/10.1029/97JD00735>
- Kurucz, R.L., Furenlid, I., Brault, J., Testerman, L. (1984). Solar flux atlas from 296 to 1300 nm. New Mexico.
- Leena, P.P., Dani, K.K., Nath, A., Sanap, S.D., Pandithurai, G., Anil Kumar, V. (2015). Validation of ground-based microwave radiometer data and its application in verifying atmospheric stability over Mahabnagar during 2011 monsoon and post-monsoon seasons. *Int. J. Remote Sens.* 36, 2920–2933. <https://doi.org/10.1080/01431161.2015.1051632>
- Levy, H. (1971). Normal atmosphere: Large radical and formaldehyde concentrations predicted. *Science* 173, 141–143. <https://doi.org/10.1126/science.173.3992.141>
- Li, X., Brauers, T., Hofzumahaus, A., Lu, K., Li, Y.P., Shao, M., Wagner, T., Wahner, A. (2013). MAX-DOAS measurements of NO₂, HCHO and CHOCHO at a rural site in Southern China. *Atmos. Chem. Phys.* 13, 2133–2151. <https://doi.org/10.5194/acp-13-2133-2013>
- Lowe, D.C., Schmidt, U. (1983). Formaldehyde (HCHO) measurements in the nonurban atmosphere. *J. Geophys. Res.* 88, 10844. <https://doi.org/10.1029/JC088iC15p10844>
- MacDonald, S.M., Oetjen, H., Mahajan, A.S., Whalley, L.K., Edwards, P.M., Heard, D.E., Jones, C.E., Plane, J.M.C. (2012). DOAS measurements of formaldehyde and glyoxal above a south-east Asian tropical rainforest. *Atmos. Chem. Phys.* 12, 5949–5962. <https://doi.org/10.5194/acp-12-5949-2012>
- Mahajan, A.S., Gómez Martín, J.C., Hay, T.D., Royer, S.J., Yvon-Lewis, S., Liu, Y., Hu, L., Prados-Roman, C., Ordóñez, C., Plane, J.M.C., Saiz-Lopez, A. (2012). Latitudinal distribution of reactive iodine in the Eastern Pacific and its link to open ocean sources. *Atmos. Chem. Phys.* 12, 11609–11617. <https://doi.org/10.5194/acp-12-11609-2012>
- Mallik, C., Lal, S. (2014). Seasonal characteristics of SO₂, NO₂, and CO emissions in and around the Indo-Gangetic Plain. *Environ. Monit. Assess.* 186, 1295–1310. <https://doi.org/10.1007/s10661-013-3458-y>
- Meller, R., Moortgat, G.K. (2000). Temperature dependence of the absorption cross sections of formaldehyde between 223 and 323 K in the wavelength range 225–375 nm. *J. Geophys. Res.* 105, 7089–7101. <https://doi.org/10.1029/1999JD901074>
- Mukherjee, S., Singla, V., Pandithurai, G., Safai, P.D., Meena, G.S., Dani, K.K., Anil Kumar, V. (2018). Seasonal variability in chemical composition and source apportionment of sub-micron aerosol over a high altitude site in Western Ghats, India. *Atmos. Environ.* 180, 79–92. <https://doi.org/10.1016/j.atmosenv.2018.02.048>
- Naja, M., Lal, S., Chand, D. (2003). Diurnal and seasonal variabilities in surface ozone at a high altitude site Mt Abu (24.6°N, 72.7°E, 1680 m asl) in India. *Atmos. Environ.* 37, 4205–4215. [https://doi.org/10.1016/S1352-2310\(03\)00565-X](https://doi.org/10.1016/S1352-2310(03)00565-X)
- Okamoto, S., Tanimoto, H. (2016). A review of atmospheric chemistry observations at mountain sites. *Prog. Earth Planet. Sci.* 3, 34. <https://doi.org/10.1186/s40645-016-0109-2>
- Petit, J.E., Favez, O., Albinet, A., Canonaco, F. (2017). A user-friendly tool for comprehensive



- evaluation of the geographical origins of atmospheric pollution: Wind and trajectory analyses. *Environ. Modell. Software* 88, 183–187. <https://doi.org/10.1016/j.envsoft.2016.11.022>
- Reddy, B.S.K., Kumar, K.R., Balakrishnaiah, G., Gopal, K.R., Reddy, R.R., Sivakumar, V., Lingaswamy, A.P., Arafath, S.M., Umadevil, K., Kumari, S.P., Ahammed, Y.N., Lal, S. (2012). Analysis of diurnal and seasonal behavior of surface ozone and its precursors (NO_x) at a semi-arid rural site in southern India. *Aerosol Air Qual. Res.* 12, 1081–1094. <https://doi.org/10.4209/aaqr.2012.03.0055>
- Renuka, K., Gadhavi, H., Jayaraman, A., Lal, S., Naja, M., Bhaskara Rao, S.V. (2014). Study of ozone and NO_2 over Gadanki - A rural site in South India. *J. Atmos. Chem.* 71, 95–112. <https://doi.org/10.1007/s10874-014-9284-y>
- Sarang, T., Naja, M., Ojha, N., Kumar, R., Lal, S., Venkataramani, S., Kumar, A., Sagar, R., Chandola, H.C. (2013). First simultaneous measurements of ozone, CO, and NO_y at a high-altitude regional representative site in the central Himalayas. *J. Geophys. Res.* 119, 1592–1611. <https://doi.org/10.1002/2013JD020631>. Received
- Sarkar, C., Chatterjee, A., Majumdar, D., Roy, A., Srivastava, A., Ghosh, S.K., Raha, S. (2017). How the atmosphere over eastern Himalaya, India is polluted with carbonyl compounds? Temporal variability and identification of sources. *Aerosol Air Qual. Res.* 17, 2206–2223. <https://doi.org/10.4209/aaqr.2017.01.0048>
- Schreier, S.F., Richter, A., Wittrock, F., Burrows, J.P. (2016). Estimates of free-Tropospheric NO_2 and HCHO mixing ratios derived from high-Altitude mountain MAX-DOAS observations at midlatitudes and in the tropics. *Atmos. Chem. Phys.* 16, 2803–2817. <https://doi.org/10.5194/acp-16-2803-2016>
- Schumann, U., Huntrieser, H. (2007). The global lightning-induced nitrogen oxides source. *Atmos. Chem. Phys.* 7, 3823–3907. <https://doi.org/10.5194/acp-7-3823-2007>
- Sinreich, R., Coburn, S., Dix, B., Volkamer, R. (2010). Ship-based detection of glyoxal over the remote tropical Pacific Ocean. *Atmos. Chem. Phys.* 10, 11359–11371. <https://doi.org/10.5194/acp-10-11359-2010>
- Smedt, I.D., Stavrakou, T., Müller, J.F., van der A, R.J., Roozendael, M.V. (2010). Trend detection in satellite observations of formaldehyde tropospheric columns. *Geophys. Res. Lett.* 37, L18808. <https://doi.org/10.1029/2010GL044245>
- Stutz, J., Kim, E.S., Platt, U. (2000). UV-visible absorption cross sections of nitrous acid. *J. Geophys. Res.* 105, 14585–14592. <https://doi.org/10.1029/2000JD900003>
- Surl, L., Palmer, P.I., González Abad, G. (2018). Which processes drive observed variations of HCHO columns over India? *Atmos. Chem. Phys.* 18, 4549–4566. <https://doi.org/10.5194/acp-18-4549-2018>
- Thalman, R., Volkamer, R. (2013). Temperature dependent absorption cross-sections of $\text{O}_2\text{-O}_2$ collision pairs between 340 and 630 nm and at atmospherically relevant pressure. *Phys. Chem. Chem. Phys.* 15, 15371–15381. <https://doi.org/10.1039/c3cp50968k>
- Vandaele, A.C., Hermans, C., Simon, P.C., Carleer, M., Colin, R., Fally, S., Merienne, M.F., Jenouvrier, A., Coquart, B. (1998). Measurements of the NO_2 absorption cross-section from 42000 cm^{-1} to 10000 cm^{-1} (238–1000 nm) at 220 K and 294 K. *J. Quant. Spectrosc. Radiat. Transfer* 59, 171–184. [https://doi.org/10.1016/S0022-4073\(97\)00168-4](https://doi.org/10.1016/S0022-4073(97)00168-4)
- Wagner, T., Dix, B., Friedeburg, C. V., Frieß, U., Sanghavi, S., Sinreich, R., Platt, U. (2004). MAX-DOAS O_4 measurements: A new technique to derive information on atmospheric aerosols—Principles and information content. *J. Geophys. Res.* 109, D22205. <https://doi.org/10.1029/2004JD004904>
- Wagner, T., Apituley, A., Beirle, S., Dörner, S., Friess, U., Remmers, J., Shaiganfar, R. (2014). Cloud detection and classification based on MAX-DOAS observations. *Atmos. Meas. Tech.* 7, 1289–1320. <https://doi.org/10.5194/amt-7-1289-2014>
- Wang, X., Wang, H., Wang, S. (2010). Ambient formaldehyde and its contributing factor to ozone and OH radical in a rural area. *Atmos. Environ.* 44, 2074–2078. <https://doi.org/10.1016/j.atmosenv.2010.03.023>
- World Health Organization (WHO) (2013). Review of evidence on health aspects of air pollution – REVIHAAP Project 309. World Health Organization.
- Zhang, R., Tie, X., Bond, D.W. (2003). Impacts of anthropogenic and natural NO_x sources over the U.S. on tropospheric chemistry. *PNAS* 100, 1505–1509. <https://doi.org/10.1073/pnas.252763799>



Zhu, L., Mickley, L.J., Jacob, D.J., Marais, E.A., Sheng, J., Hu, L., Abad, G.G., Chance, K. (2017). Long-term (2005–2014) trends in formaldehyde (HCHO) columns across North America as seen by the OMI satellite instrument: Evidence of changing emissions of volatile organic compounds. *Geophys. Res. Lett.* 44, 7079–7086. <https://doi.org/10.1002/2017GL073859>